Available online at www.sciencedirect.com
SCIENCE DIRECT®
Journal of Computational Physics 206 (2005) 559–577
JOURNAL OF COMPUTATIONAL PHYSICS
www.elsevier.com/locate/jcp

A global semi-Lagrangian spectral model of the shallow water equations with variable resolution

Daniel X. Guo [a,*], John B. Drake [b]

[a] *Department of Mathematics and Statistics, University of North Carolina at Wilmington, 601 South College Road, Wilmington, NC 28403-3297, USA*
[b] *Computer Science and Mathematics Division, Oak Ridge National Laboratory, Oak Ridge, TN 37831, USA*

Received 1 July 2004; received in revised form 22 December 2004; accepted 22 December 2004
Available online 12 February 2005

Abstract

A new formulation of a semi-implicit, semi-Lagrangian spectral method is given together with a conformal mapping of the underlying Gaussian grid. The mapping based on the Schmidt transformation focuses grid resolution on a particular region. The advective form of the vorticity–divergence equations allows the conformal map to be incorporated in a semi-Lagrangian transport step while maintaining an efficient spectral transform algorithm. The shallow water equations on the sphere are solved to test the variable resolution spectral model. By focusing on a specified location, local details of the flow are more accurately resolved. Accuracy and stability of the method are compared with uniform spectral solutions.

Keywords: Semi-Lagrangian; Spectral; Conformal transformation; Variable resolution; Shallow water equations

1. Introduction

Smooth grid transformations in spectral atmospheric models were introduced in Schmidt's pioneering paper [13]. He defined a conformal mapping of the sphere onto itself with the property that the spherical Laplacian and Jacobian in the mapped coordinate system are simply modified by a mapping factor. This leads to an elegant Eulerian formulation of the shallow water equations and can be used as a basis for numerical approximations and numerical solutions with high resolution in a particular focused area. A number of authors have used the Schmidt transformation with Eulerian numerical schemes in the shallow water equation context [2,8,14]. Coutier and Geleyn [2] did not extend the mapping to the solution of the

* Corresponding author. Tel.: +1 910 962 3671; fax: +1 910 962 7107.
E-mail address: guod@uncw.edu (D.X. Guo).

0021-9991/$ - see front matter
doi:10.1016/j.jcp.2004.12.020

semi-implicit equations in spectral space and introduced an approximate solution only valid for Eulerian models. This was extended in the multi-level operational weather forecasting system ARPEGE/IFS [21] to integrate the mapping factor in the spectral part of the calculation and, in particular, appears in the solution of the semi-implicit Helmholtz equation by a penta-diagonal matrix solve in spectral space. This system has been used to provide local area forecasts operationally. It is reported in [4] that a T63 model with stretching ($c = 3.5$) produces better accuracy in a 10-year European climate simulation than the uniform T106 spectral model.

The advection term can be treated in grid point space independently of the spectral space approximations. The semi-Lagrangian transport (SLT) method is used in atmospheric general circulation models to advect mass, momentum, energy and chemical species [10,11,15,20,21]. The method updates the value of a field at a grid point by first establishing a trajectory through which the particle has moved during the current timestep. This trajectory is found iteratively using the interpolated velocity field at the midpoint of the trajectory. The field value is interpolated at the departure point using shape preserving interpolation.

Williamson's SLT formulation in [20] used vorticity–divergence variables derived by taking the curl and divergence of the discrete semi-Lagrangian momentum equation. In this formulation, the non-advective terms are discretized using a spherical harmonic transform to approximate the spatial derivatives and solve a Helmholtz equation arising from the semi-implicit time stepping. First and second order spatial derivative terms are lumped together making it difficult to incorporate the Schmidt transformation in the spectral transform. The improvement offered in [5,6] is that only the Laplacian operator appears in the mapped equations and the SLT discretization is applied directly to the scalar advective form of the vorticity/divergence equations. The present paper extends the formulation to incorporate the Schmidt transformation in the advective formulation of the shallow water equations in spherical geometry. Extension to multi-level baroclinic models should be straightforward.

The semi-Lagrangian method combined with spectral approximation is a powerful algorithm. The high accuracy obtained for the approximation of spatial derivatives and the ease of solution for a semi-implicit system that filters the fast gravity wave terms make this algorithm competitive in accuracy and computational efficiency. Treating the non-linear advective terms with the semi-Lagrangian transport removes the Courant limits, allowing long time steps while maintaining stability and shape [18]. It is found that local accuracy can be enhanced while maintaining stability in the context of long time steps. No horizontal diffusion operators were needed to damp high frequency waves since there is inherent smoothing in the semi-Lagrangian interpolation. An Asselin time filter was necessary, however, to suppress the spurious computational mode of the three time level centered differences. The accuracy and stability properties of the variable resolution spectral approximations are tested using some of the standard shallow water test cases given in [19].

2. Shallow water equations and model equations on the sphere

The shallow water equations in advective form [19] in spherical geometry are

$$\frac{\mathrm{d}\mathbf{v}}{\mathrm{d}t} = -f\vec{k} \times \mathbf{v} - \nabla\phi, \tag{1}$$

$$\frac{\mathrm{d}\phi^*}{\mathrm{d}t} = -\phi^* \nabla \cdot \mathbf{v}, \tag{2}$$

where $\mathbf{v} = u\vec{i} + v\vec{j}$, the horizontal velocity, is orthogonal to the unit vector $\vec{k}$ in the radial direction. The free surface geopotential is denoted by $\phi = \phi^* + \phi_s = g(h^* + h_s)$ and $\phi^* = \phi' + \bar{\phi}$, where g is the gravitational acceleration and h^* is the height of the free surface above the bottom height, h_s. The bottom surface height specifies orography as a time invariant function and $\bar{\phi}$ is the time invariant spatial mean. The Coriolis term,

$f = 2\Omega \sin\theta$, incorporates the rotation effects at latitude θ of the sphere with angular velocity Ω. The normalized substantial derivative is given by

$$\frac{\mathrm{d}}{\mathrm{d}t} = \frac{\partial}{\partial t} + \mathbf{v} \cdot \nabla.$$

Eqs. (1) and (2) require no boundary conditions but are posed with initial conditions on $\mathbf{v}$ and ϕ.

To avoid problems with the vector representation of the velocity at the poles and to maintain compatibility with the scalar spectral transform method, the equations can be written in terms of the vorticity $\zeta \equiv \vec{k} \cdot \nabla \times \mathbf{v}$ and divergence $\delta \equiv \nabla \cdot \mathbf{v}$.

Two identities for spherical geometry are needed to derive the vorticity and divergence form,

$$(\mathbf{v} \cdot \nabla)\mathbf{v} \equiv \nabla\left(\frac{\mathbf{v} \cdot \mathbf{v}}{2}\right) + \zeta\vec{k} \times \mathbf{v}$$

and

$$\nabla \times (\nabla \times \mathbf{v}) = \nabla(\nabla \cdot \mathbf{v}) - \frac{1}{\cos\theta}\nabla^2(\mathbf{v}\cos\theta) - \frac{2\sin\theta}{a\cos\theta}F,$$

where

$$F = \begin{pmatrix} -\zeta \\ \delta \end{pmatrix}.$$

By applying $\vec{k} \cdot \nabla\times$ and divergence operator $\nabla\cdot$ to (1) we obtain the advective form of the vorticity and divergence equations

$$\frac{\mathrm{d}\eta}{\mathrm{d}t} = -\eta\delta, \tag{3}$$

$$\frac{\mathrm{d}\delta}{\mathrm{d}t} + \nabla^2\phi^* = \Psi, \tag{4}$$

where

$$\Psi = \eta(\eta - f) - \vec{k} \cdot \mathbf{v} \times \nabla f + \mathbf{v} \cdot \tilde{F} - \nabla^2\left(\phi_s + \frac{\mathbf{v} \cdot \mathbf{v}}{2}\right), \tag{5}$$

$$\tilde{F} = \frac{1}{\cos\theta}\nabla^2(\mathbf{v}\cos\theta) + \frac{2\sin\theta}{a\cos\theta}F, \tag{6}$$

and

$$\eta = \zeta + f.$$

To obtain $\mathbf{v}$ from ζ and δ, the Helmholtz theorem separates the horizontal velocity vector $\mathbf{v}$ into a scalar stream function ψ and a scalar velocity potential χ, as

$$\mathbf{v} = \vec{k} \times \nabla\psi + \nabla\chi. \tag{7}$$

Application of the curl and divergence operators to (7) gives the relationships for the prognostic variables ζ and δ in terms of the stream function and the velocity potential

$$\nabla^2\psi = \zeta,$$

and

$$\nabla^2\chi = \delta.$$

The prognostic equations for vorticity (3) and divergence (4) involve only the Laplacian operator and the advective operator in the left-hand sides. This form is useful because of its simple differential structure. Avoiding the first derivative has distinct advantages for the smooth grid mappings to be investigated. The details of the derivation are given in [5].

3. Schmidt's conformal transformation

The results in this section follow [2,13]. Consider a mapping L of the sphere to itself defined by

$$(\lambda', \mu') = L(\lambda, \mu),$$

where $\mu = \sin\theta$ and λ and θ are the spherical coordinates, longitude and latitude, respectively; (λ', μ') are the transformed coordinates. For functions g, g' with spherical domain a prime indicates the dependence on the new coordinates λ' and μ'. The new coordinates define the sphere in what we will call "physical space" and will be the site of a mapped, variable resolution grid.

Let $F'(\lambda', \mu')$, the so-called mapping factor, be the determinant of the Jacobian matrix of the mapping L,

$$F'(\lambda', \mu') = \begin{vmatrix} \frac{\partial \lambda'}{\partial \lambda} & \frac{\partial \mu'}{\partial \lambda} \\ \frac{\partial \lambda'}{\partial \mu} & \frac{\partial \mu'}{\partial \mu} \end{vmatrix} = \begin{vmatrix} \frac{\partial \lambda}{\partial \lambda'} & \frac{\partial \mu}{\partial \lambda'} \\ \frac{\partial \lambda}{\partial \mu'} & \frac{\partial \mu}{\partial \mu'} \end{vmatrix}^{-1}.$$

For the shallow water equations, the spectral method using a collocation grid and truncation without aliasing errors has the spectral closure property. The closure property is that if the vorticity, divergence and geopotential are expressed in a finite series of spherical harmonics, then the tendencies of those fields produced by the discrete equations are a finite series of spherical harmonics. This property is conserved in the shallow water equations transformed by a conformal mapping (the fields and the Coriolis parameter being expressed in a finite series of spherical harmonics defined over the mapped sphere) if and only if the function $F'(\lambda', \mu')$ has a decomposition in a finite set of spherical harmonics of the mapped sphere. The mapping L is then said to be spectral.

If L is a conformal mapping, then we have a property as expressed by Schmidt [13],

$$\nabla^2 A = F'(\lambda', \mu') \nabla'^2 A', \tag{8}$$

where ∇'^2 is the standard Laplacian operator with respect to the transformed coordinates (λ', μ') and A is a scalar function.

We introduce two transformations, rotation and stretching, that after transformation, locate the finest resolution grid at some specified location.

3.1. Rotation

Let R be a rotation transformation. $P(\lambda_0, \theta_0)$ is a given point on the unit sphere as illustrated in Fig. 1. After applying the rotation R, one of the new coordinate axes will go thorough this point. The equations of the rotation that relate the two coordinate systems are

$$\begin{aligned} &\cos\theta' \sin(\lambda' - \lambda_0) = \cos\theta \sin(\lambda - \lambda_0), \\ &\cos\theta' \cos(\lambda' - \lambda_0) = \cos\theta \cos(\lambda - \lambda_0) \sin\theta_0 + \sin\theta \cos\theta_0, \\ &\sin\theta' = -\cos\theta \cos(\lambda - \lambda_0) \cos\theta_0 + \sin\theta \sin\theta_0. \end{aligned} \tag{9}$$

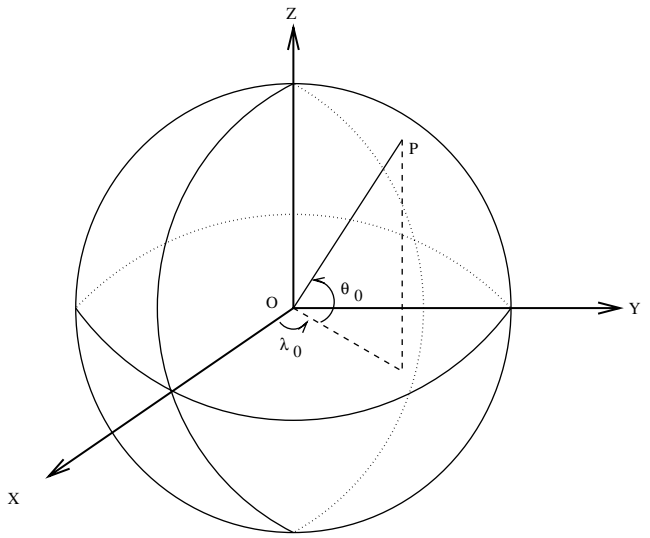

Fig. 1. A point $P(\lambda_0, \theta_0)$ on the unit sphere in lat–lon coordinates.

The inverse transformation, obtained by direct computation, is

$$\begin{aligned}
&\cos\theta\sin(\lambda-\lambda_0) = \cos\theta'\sin(\lambda'-\lambda_0),\\
&\cos\theta\cos(\lambda-\lambda_0) = \cos\theta'\cos(\lambda'-\lambda_0)\sin\theta_0 - \sin\theta'\cos\theta_0,\\
&\sin\theta = \cos\theta'\cos(\lambda'-\lambda_0)\cos\theta_0 + \sin\theta'\sin\theta_0.
\end{aligned} \tag{10}$$

Again by direct computation, the Jacobian of the transformation involves the partial derivatives

$$\begin{aligned}
\frac{\partial\lambda}{\partial\lambda'} &= \frac{\cos^2\theta'\sin\theta_0 - \cos\theta'\sin\theta'\cos(\lambda'-\lambda_0)\cos\theta_0}{\cos^2\theta},\\
\frac{\partial\lambda}{\partial\mu'} &= \frac{\sin(\lambda'-\lambda_0)\cos\theta_0}{\cos\theta'\cos^2\theta},\\
\frac{\partial\mu}{\partial\lambda'} &= -\cos\theta'\sin(\lambda'-\lambda_0)\cos\theta_0,\\
\frac{\partial\mu}{\partial\mu'} &= \frac{-\sin\theta'\cos(\lambda'-\lambda_0)\cos\theta_0 + \cos\theta'\sin\theta_0}{\cos\theta'}.
\end{aligned} \tag{11}$$

If $\theta = \pm\pi/2$, then $\partial\lambda/\partial\mu'$ and $\partial\mu/\partial\mu'$ are undefined. By changing the stretching factor such that there is no grid point located at the poles, this problem can be avoided without adding any restrictions on the focusing area and stretching factor.

The mapping factor of the rotation R is

$$F'_R(\lambda', \mu') = 1$$

and hence the rotation is spectral.

3.2. Stretching

Let S be a stretching transformation given by

$$\lambda' = \lambda,$$
$$\mu' = \frac{(c^2-1)+\mu(c^2+1)}{(c^2+1)+\mu(c^2-1)}, \tag{12}$$

where c is the stretching factor. Depending on the value of c (>1 or <1), we stretch the mesh towards the north pole or the south pole. The inverse transformation is obtained for c^{-1}, it is,

$$\lambda = \lambda',$$
$$\mu = \frac{-(c^2-1)+\mu'(c^2+1)}{(c^2+1)-\mu'(c^2-1)}. \tag{13}$$

The partial derivatives in the Jacobian are

$$\begin{aligned} &\partial\lambda/\partial\lambda' = 1, \quad \partial\lambda/\partial\mu' = 0, \quad \partial\mu/\partial\lambda' = 0, \\ &\partial\mu/\partial\mu' = 4c^2/\{c^2+1-\mu'(c^2-1)\}^2 \end{aligned} \tag{14}$$

and the mapping factor of S is then,

$$F'_S(\lambda',\mu') = \{c^2+1-\mu'(c^2-1)\}^2/4c^2. \tag{15}$$

The stretching transformation S is also spectral.

In order to put the finest grids on a specified region, we need to combine the stretching and the rotation transformations. So define the mapping L as the product of the mapping R and S. The mapping factor $F'(\lambda',\mu')$ of L is given by

$$F'(\lambda',\mu') = F'_R(\lambda',\mu')\cdot F'_S(\lambda',\mu') = \left\{\frac{c^2+1}{2c} - \frac{c^2-1}{2c}\mu'\right\}^2. \tag{16}$$

The mapping factor $F'(\lambda',\mu')$ of L is a second-order polynomial in μ' and hence the mapping is spectral.

Once a discrete Gaussian grid is introduced for the spectral transformations, the effect of the mapping will be to focus points near the pole and rotate this focused pole to an area of interest and high resolution.

4. Semi-Lagrangian formulation

A three time level SLT method for the shallow water equations was described in [11]. For meteorological models, the form of the method is based on a division of terms in the equations between those involved in the fast moving gravity waves and the slower moving Rossby waves. A trapezoidal rule is used to integrate the fast terms and a spatially averaged mid-point rule is used for the slow terms. All the calculations for the SLT are performed in the physical space of the mapped grid with coordinates. The interpolations are performed on a non-uniform, tensor product grid.

The semi-implicit, semi-Lagrangian scheme for the shallow water model in vorticity–divergence takes the form

$$\eta_A^{\tau+1} = N_\eta, \tag{17}$$

$$\delta_A^{\tau+1} + \Delta t[\nabla^2\phi]_A^{\tau+1} = N_\delta, \tag{18}$$

$$\phi_A^{\tau+1} + \Delta t[\bar{\phi}\delta]_A^{\tau+1} = N_\phi, \tag{19}$$

where $N = (N_\eta, N_\delta, N_\phi)^{\mathrm{T}}$ and $N = N_{\mathrm{A}} + N_{\mathrm{D}}$, the arrival and departure components of N, are defined by

$$N_{\mathrm{A}} = \begin{pmatrix} -\Delta t[\eta\delta]_A^{\tau} \\ \Delta t[\Psi]_A^{\tau} \\ -\Delta t[\phi\delta]_A^{\tau} \end{pmatrix}, \tag{20}$$

and

$$N_{\mathrm{D}} = \begin{pmatrix} \eta_D^{\tau-1} - \Delta t[\eta\delta]_D^{\tau} \\ \delta_D^{\tau-1} + \Delta t[\Psi]_D^{\tau} - \Delta t[\nabla^2\phi]_D^{\tau-1} \\ \phi_D^{\tau-1} - \Delta t[\phi\delta]_D^{\tau} - \Delta t[\bar{\phi}\delta]_D^{\tau-1} \end{pmatrix}. \tag{21}$$

For the details of the derivation and variants of this scheme, see [5].

The quantities $\mathbf{v}^{\tau}$, η^{τ}, δ^{τ}, ϕ^{τ}, $\eta^{\tau-1}$, $\delta^{\tau-1}$, $\phi^{\tau-1}$ and $\nabla^2(\mathbf{v}\cdot\mathbf{v})^{\tau}$, $\nabla^2\phi^{\tau-1}$ are evaluated at the departure points in physical space. These quantities are used to form N_{D}. Alternatively, the sums of terms involved in N_{D} can be formed at the grid points and then interpolated to the departure points. This is computationally less expensive and introduces an error only on the order of the interpolation error. The interpolations are shape preserving using a tensor product cubic interpolation scheme developed by Williamson and Rasch [18].

The departure point calculation integrates the equation

$$\frac{\mathrm{d}\mathbf{x}}{\mathrm{d}t} = \mathbf{v}$$

backwards in time along the trajectory from the arrival point. Previous work [15] indicates that a linear interpolation in the calculation of the trajectories is adequate for accuracy in the solution of the shallow water equations. To avoid the singularity at the poles of the velocity field, a three-dimensional technique is used [1,11]. The two-dimensional vectors on the sphere are lifted to three-dimensional vectors in Cartesian coordinates. A Lagrange cubic interpolation is used for velocities.

5. Spectral semi-implicit formulation

The semi-implicit formulation for numerical weather prediction has been standard since its introduction by Robert et al. [12]. The combination of the semi-Lagrangian method with the spectral transform method has proven to be a powerful technique, providing easy solution of the Helmholtz equation resulting from the semi-implicit formulation, high spatial accuracy and long timesteps. In addition, Cote and Staniforth [3] have observed that the semi-Lagrangian treatment of the advection eliminates the nonlinear aliasing of terms in the spectral representation allowing use of more terms of the spectral expansion with the same physical grid and effectively doubling the resolution at little extra cost.

The spectral transform, or more correctly, the spherical harmonic transform, is based on the representation of scalar fields as a linear combination of spherical harmonics as

$$\xi(\lambda,\mu) = \sum_{m=-M}^{M} \sum_{n=|m|}^{N(m)} \xi_n^m P_n^m(\mu) \mathrm{e}^{\mathbf{i}m\lambda} \tag{22}$$

with

$$\xi_n^m = \int_{-1}^{1} \frac{1}{2\pi} \int_0^{2\pi} \xi(\lambda,\mu) \mathrm{e}^{-\mathbf{i}m\lambda}\, \mathrm{d}\lambda P_n^m(\mu)\, \mathrm{d}\mu, \tag{23}$$

where P_n^m are the normalized associated Legendre functions. (For more details of the associated Legendre functions see [16] or Appendix B in [17].)

All the spectral transforms are computed on a uniform Gaussian grid. This is the grid that is mapped to the variable resolution, physical space grid. It is necessary to use this Gaussian grid to exactly calculate the spectral coefficients using a Gaussian quadrature. Once spectral coefficients are known, the transformation from spectral to the uniform grid space is accomplished using (22) and is referred to as harmonic synthesis. The transform from physical space to spectral space (harmonic analysis) uses a discrete version of the continuous transform

$$\xi^m(\mu) = \frac{1}{2\pi}\int_0^{2\pi} \xi(\lambda,\mu)\mathrm{e}^{-\mathbf{i}m\lambda}\,\mathrm{d}\lambda P_n^m(\mu)\,\mathrm{d}\mu = \frac{1}{I}\sum_{i=1}^{I}\xi(\lambda_i,\mu)\mathrm{e}^{-\mathbf{i}m\lambda_i}, \tag{24}$$

and

$$\xi_n^m = \int_{-1}^{+1}\xi^m(\mu)P_n^m(\mu)\,\mathrm{d}\mu = \sum_{j=1}^{J}\xi^m(\mu_j)P_n^m(\mu_j)w_j, \tag{25}$$

where

$$\lambda_i = \frac{2\pi i}{I}, \quad w_j = \frac{2(1-\mu_j^2)}{[JP_{J-1}(\mu_j)]^2}, \quad \sum_{j=1}^{J} w_j = 2,$$

and μ_j denote the Gaussian latitudes; I is the number of gridpoints in the east–west direction; J the number of Gaussian latitudes from pole to pole; w_j the Gaussian weight at latitude μ_j; the Gaussian latitudes μ_j are determined from the roots of the Legendre polynomial $P_J(\mu)$.

By introducing a conformal mapping L and applying the property of conformal mapping given in (8), we obtain the transformed equations from (17)–(19) as follows:

$$[\eta]_A^{\tau+1} = N_\eta, \tag{26}$$

$$[\delta]_A^{\tau+1} + \Delta t[\nabla^2\phi F]_A^{\tau+1} = N_\delta, \tag{27}$$

$$[\phi]_A^{\tau+1} + \Delta t[\bar{\phi}\delta]_A^{\tau+1} = N_\phi, \tag{28}$$

where

$$\begin{aligned} N_\eta &\equiv [\eta]_D^{\tau-1} - \Delta t\{[\eta\delta]_A^{\tau} + [\eta\delta]_D^{\tau}\},\\ N_\delta &\equiv [\delta]_D^{\tau-1} + \Delta t\{[\Psi]_A^{\tau} + [\Psi]_D^{\tau} - [\Delta\phi]_D^{\tau-1}\},\\ N_\phi &\equiv [\phi]_D^{\tau-1} - \Delta t\{[\phi\delta]_A^{\tau} + [\phi\delta]_D^{\tau} + [\bar{\phi}\delta]_D^{\tau-1}\} \end{aligned} \tag{29}$$

and Ψ is defined in (5). For simplicity all primes have been dropped.

Applying the transformation given in (23) to each term of Eqs. (26)–(28) only three types of terms result: the terms involving unknowns with constant coefficients, the terms involving unknowns with a Laplacian operator, and the rest. Transformation of the terms with constant coefficients are obtained by direct application of (24) and (25).

For terms of N_η, N_δ, and N_ϕ, we need $\eta^{\tau-1}$, $\delta^{\tau-1}$, $\phi^{\tau-1}$, η^τ, δ^τ, ϕ^τ, $\mathbf{v}^\tau$, and $[\nabla^2\phi F]^\tau$ at the arrival points on physical space. By using high order interpolation to obtain their values at the departure-point on the same space, then we are able to use Eqs. (24) and (25) to compute $\{N_\eta\}_n^m$, $\{N_\delta\}_n^m$, and $\{N_\phi\}_n^m$ on spectral space.

Finally, for the term with a Laplacian operator we will use a property of associated Legendre functions on spectral space [21]

$$\mu P_n^m = e_n^m P_{n-1}^m + e_{n+1}^m P_{n+1}^m,$$

where n and m are the total and zonal wave numbers, respectively, and

$$e_n^m = \begin{cases} \sqrt{(n^2-m^2)/(4n^2-1)} & \text{for } |m| \leqslant n, \\ 0 & \text{for } |m| > n. \end{cases}$$

Let

$$\alpha = \frac{c^2+1}{2c}, \quad \beta = \frac{c^2-1}{2c},$$

we then obtain $F(\lambda,\mu) = (\alpha + \beta\mu)^2$ and

$$FP_n^m = c_{-2,n}^m P_{n-2}^m + c_{-1,n}^m P_{n-1}^m + c_{0,n}^m P_n^m + c_{1,n}^m P_{n+1}^m + c_{2,n}^m P_{n+2}^m, \tag{30}$$

where

$$\begin{aligned} c_{-2,n}^m &= \beta^2 e_n^m e_{n-1}^m, \\ c_{-1,n}^m &= 2\alpha\beta e_n^m, \\ c_{0,n}^m &= \alpha^2 + \beta^2 e_n^m e_n^m + \beta^2 e_{n+1}^m e_{n+1}^m, \\ c_{1,n}^m &= 2\alpha\beta e_{n+1}^m, \\ c_{2,n}^m &= \beta^2 e_{n+1}^m e_{n+2}^m. \end{aligned} \tag{31}$$

Applying sequential integration by parts and the relationship

$$\nabla^2 P_n^m(\mu)\mathrm{e}^{\mathrm{i}m\lambda} = \frac{-n(n+1)}{a^2} P_n^m(\mu)\mathrm{e}^{im\lambda},$$

to the term with a Laplacian operator such that

$$\begin{aligned} \{\nabla^2\phi F\}_n^m &= \int_{-1}^{+1} \frac{1}{2\pi} \int_0^{2\pi} \nabla^2(\phi F)\mathrm{e}^{\mathrm{i}m\lambda}\,\mathrm{d}\lambda P_n^m(\mu)\,\mathrm{d}\mu \\ &= \int_{-1}^{+1} \frac{1}{2\pi} \int_0^{2\pi} \nabla^2\phi(FP_n^m(\mu))\mathrm{e}^{\mathrm{i}m\lambda}\,\mathrm{d}\lambda\,\mathrm{d}\mu \\ &= \int_{-1}^{+1} \frac{1}{2\pi} \int_0^{2\pi} \nabla^2\phi(c_{-2,n}^m P_{n-2}^m + c_{-1,n}^m P_{n-1}^m + c_{0,n}^m P_n^m + c_{1,n}^m P_{n+1}^m + c_{2,n}^m P_{n+2}^m)\mathrm{e}^{\mathrm{i}m\lambda}\,\mathrm{d}\lambda\,\mathrm{d}\mu \\ &= \int_{-1}^{+1} \frac{1}{2\pi} \int_0^{2\pi} \phi\mathrm{e}^{\mathrm{i}m\lambda}\,\mathrm{d}\lambda(d_{-2,n}^m P_{n-2}^m + d_{-1,n}^m P_{n-1}^m + d_{0,n}^m P_n^m + d_{1,n}^m P_{n+1}^m + d_{2,n}^m P_{n+2}^m)\,\mathrm{d}\mu \\ &= d_{-2,n}^m \phi_{n-2}^m + d_{-1,n}^m \phi_{n-1}^m + d_{0,n}^m \phi_n^m + d_{1,n}^m \phi_{n+1}^m + d_{2,n}^m \phi_{n+2}^m, \end{aligned} \tag{32}$$

where

$$\begin{aligned} d_{-2,n}^m &= \frac{-(n-2)(n-1)}{a^2} c_{-2,n}^m, \\ d_{-1,n}^m &= \frac{-(n-1)n}{a^2} c_{-1,n}^m, \\ d_{0,n}^m &= \frac{-n(n+1)}{a^2} c_{0,n}^m, \\ d_{1,n}^m &= \frac{-(n+1)(n+2)}{a^2} c_{1,n}^m, \\ d_{2,n}^m &= \frac{-(n+2)(n+3)}{a^2} c_{2,n}^m \end{aligned} \tag{33}$$

and a is the radius of the earth.

For simplicity we drop the index $\tau + 1$ and the subscript A to obtain the spectral form of the governing equations

$$\{\eta\}_n^m = \{N_\eta\}_n^m, \tag{34}$$

$$\{\delta\}_n^m + \Delta t\{d_{-2,n}^m\{\phi\}_{n-2}^m + d_{-1,n}^m\{\phi\}_{n-1}^m + d_{0,n}^m\{\phi\}_n^m + d_{1,n}^m\{\phi\}_{n+1}^m + d_{2,n}^m\{\phi\}_{n+2}^m\} = \{N_\delta\}_n^m, \tag{35}$$

and

$$\{\phi\}_n^m + \Delta t\bar{\phi}\{\delta\}_n^m = \{N_\phi\}_n^m. \tag{36}$$

The spectral coefficient of vorticity $\{\eta\}_n^m$ is obtained directly from Eq. (34). Eqs. (35) and (36) must be solved simultaneously in spectral space. The solution of this two by two system yields a semi-implicit treatment of the fast wave terms and a trivial implicit solution cost. This essential feature of the spectral semi-implicit algorithm described in [7] is thus preserved in the current algorithm.

Let $c_{\Delta t} = (\Delta t)^2\bar{\phi}$. By substituting Eq. (36) into Eq. (35) the general equation of the system is

$$\begin{aligned} &-c_{\Delta t}d_{-2,n}^m\{\phi\}_{n-2}^m - c_{\Delta t}d_{-1,n}^m\{\phi\}_{n-1}^m + (1 - c_{\Delta t}d_{0,n}^m)\{\phi\}_n^m - c_{\Delta t}d_{1,n}^m\{\phi\}_{n+1}^m - c_{\Delta t}d_{2,n}^m\{\phi\}_{n+2}^m \\ &\quad = \{N_\phi\}_n^m - \Delta t\bar{\phi}\{N_\delta\}_n^m \end{aligned} \tag{37}$$

for all m and n.

Eq. (37) is not coupled in m, so for a given m, we can solve a linear system with a penta-diagonal matrix for $\{\phi\}_n^m$, $n = |m|, \ldots, N$, where N is defined in (22). For a given m, we have $N - m + 1$ equations and $N - m + 3$ unknowns. The spectral truncation gives the closure conditions

$$\{\phi\}_{N+1}^m = \{\phi\}_{N+2}^m = 0 \quad \text{for all } m.$$

From the spectral transform defined in (22), all functions are projected on the spectral space by truncating to the term $N(m)$ or N. So, this closure will not have any effect on the truncation errors.

To recover $\mathbf{v}$ from η and δ use (11) and (12) to obtain

$$F\nabla^2\psi = \zeta, \quad F\nabla^2\chi = \delta.$$

Repeating the same process with a transformed Laplacian operator, the spectral forms are

$$d_{-2,n}^m\{\psi\}_{n-2}^m + d_{-1,n}^m\{\psi\}_{n-1}^m + d_{0,n}^m\{\psi\}_n^m + d_{1,n}^m\{\psi\}_{n+1}^m + d_{2,n}^m\{\psi\}_{n+2}^m\} = \{\zeta\}_n^m, \tag{38}$$

and

$$d_{-2,n}^m\{\chi\}_{n-2}^m + d_{-1,n}^m\{\chi\}_{n-1}^m + d_{0,n}^m\{\chi\}_n^m + d_{1,n}^m\{\chi\}_{n+1}^m + d_{2,n}^m\{\chi\}_{n+2}^m\} = \{\delta\}_n^m. \tag{39}$$

To compute $\{\psi\}_{N+1}^m$, $\{\psi\}_{N+2}^m$, and $\{\chi\}_{N+1}^m$, $\{\chi\}_{N+2}^m$, the same closure from the spectral truncation is used. The velocity potential and stream function in physical space are obtained from the synthesis of the transform (22)

$$\psi(\lambda, \mu) = \sum_{m=-M}^{M}\sum_{n=|m|}^{N(m)}\psi_n^m P_n^m(\mu)\mathrm{e}^{\mathrm{i}m\lambda}, \tag{40}$$

and

$$\chi(\lambda, \mu) = \sum_{m=-M}^{M}\sum_{n=|m|}^{N(m)}\chi_n^m P_n^m(\mu)\mathrm{e}^{\mathrm{i}m\lambda}. \tag{41}$$

The first order derivatives are given by the synthesis formulas:

$$\frac{\partial\psi(\lambda,\mu)}{\partial\lambda}=\sum_{m=-M}^{M}\sum_{n=|m|}^{N(m)}\mathbf{i}m\psi_n^m P_n^m(\mu)\mathrm{e}^{\mathbf{i}m\lambda}, \tag{42}$$

$$\frac{\partial\psi(\lambda,\mu)}{\partial\mu}=\sum_{m=-M}^{M}\sum_{n=|m|}^{N(m)}\psi_n^m\frac{\mathrm{d}P_n^m(\mu)}{\mathrm{d}\mu}\mathrm{e}^{\mathbf{i}m\lambda}, \tag{43}$$

$$\frac{\partial\chi(\lambda,\mu)}{\partial\lambda}=\sum_{m=-M}^{M}\sum_{n=|m|}^{N(m)}\mathbf{i}m\chi_n^m P_n^m(\mu)\mathrm{e}^{\mathbf{i}m\lambda}, \tag{44}$$

$$\frac{\partial\chi(\lambda,\mu)}{\partial\mu}=\sum_{m=-M}^{M}\sum_{n=|m|}^{N(m)}\chi_n^m\frac{\mathrm{d}P_n^m(\mu)}{\mathrm{d}\mu}\mathrm{e}^{\mathbf{i}m\lambda}. \tag{45}$$

To avoid any confusion, we put the primes back on the variables as

$$\frac{\partial\psi'}{\partial\lambda'},\quad\frac{\partial\psi'}{\partial\mu'},\quad\frac{\partial\chi'}{\partial\lambda'},\quad\frac{\partial\chi'}{\partial\mu'}.$$

The velocities U' and V' are obtained from from Eq. (7). Changing the coordinates we obtain

$$U'=\frac{1}{a}\left(\frac{\partial\chi'}{\partial\lambda'}\frac{\partial\lambda'}{\partial\lambda}+\frac{\partial\chi'}{\partial\mu'}\frac{\partial\mu'}{\partial\lambda}\right)-\frac{1-\mu(\lambda',\mu')^2}{a}\left(\frac{\partial\psi'}{\partial\lambda'}\frac{\partial\lambda'}{\partial\mu}+\frac{\partial\psi'}{\partial\mu'}\frac{\partial\mu'}{\partial\mu}\right), \tag{46}$$

and

$$V'=\frac{1}{a}\left(\frac{\partial\psi'}{\partial\lambda'}\frac{\partial\lambda'}{\partial\lambda}+\frac{\partial\psi'}{\partial\mu'}\frac{\partial\mu'}{\partial\lambda}\right)+\frac{1-\mu(\lambda',\mu')^2}{a}\left(\frac{\partial\chi'}{\partial\lambda'}\frac{\partial\lambda'}{\partial\mu}+\frac{\partial\chi'}{\partial\mu'}\frac{\partial\mu'}{\partial\mu}\right). \tag{47}$$

6. Numerical experiments and results

In this section, we compare the numerical results from two of the standard test cases described in [19] with numerical solutions presented in [9] from an Eulerian spectral model. All results are based on the T42 mesh with different stretching factors, and with the focal point located at $(3\pi/2,\pi/6)$, as shown in Fig. 2 for $c=3$, $\lambda_0=3\pi/2$ and $\theta_0=7\pi/36$. A time step of $\Delta t=1200$ s was used for the simulations. In order to compare solutions from the stretched and unstretched grids, interpolation is performed to a uniform grid.

6.1. Advection test

With $\alpha=\pi-0.05$, the cosine bell is advected over the poles at a slight offset. The initial height field should be maintained throughout the course of one twelve-day rotation, but because of the numerical approximation, the peak erodes. Fig. 3 shows the results after two days, eight days and one rotation twelve days. The viewpoint is set at the center of the cosine bell so the focal point appears in the center of the plot. The plot on the left shows the error of the height field on the stretched ($c=2$) and rotated $(3\pi/2,\pi/6)$ grids while the right on the regular grids. Clearly, the accuracy is better with the stretched ($c=2$) grid at day two (Fig. 3(a)). The solution also appears smoother with fewer oscillations in front of and behind the bell.

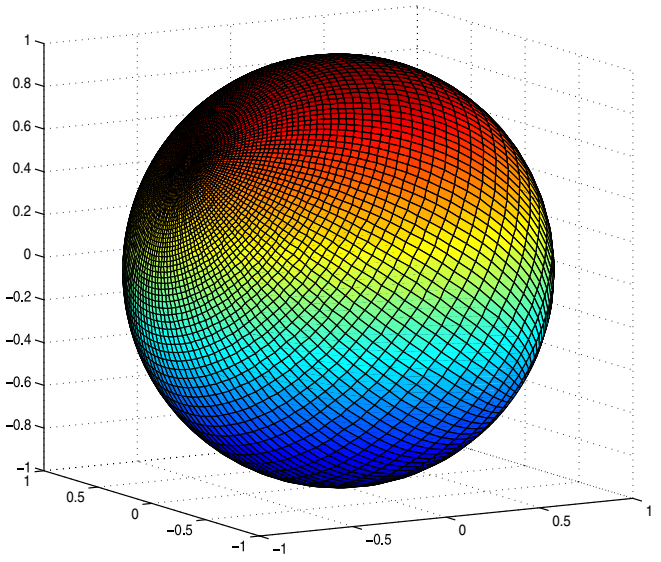

Fig. 2. T42 mesh after stretching ($c = 3$) and rotation to $(3\pi/2, 7\pi/36)$.

This is what one expects, and hopes for, with the added resolution of the focused grid. The semi-Lagrangian transport method applied only to the geopotential equation does not exercise the entire algorithm. What is exercised is primarily the interpolation on the stretched grid in the reconstruction of the old time level height field at departure points. The smaller grid spacing increases the spatial accuracy of the interpolation yielding more accurate results. When the bell advects out of the focused region, the mesh spacing increases as does the interpolation error. Fig. 3(b) shows the solution at day eight when the cosine bell is located on the coarsest part of the mesh, on the opposite side of the sphere from the focal point. The plot is viewed from directly above this location and the error is now larger than the unstretched solution at the same time. Oscillations before and after have developed in the same pattern as the unstretched regular grid solution.

The final height field error after one rotation (12 days or 864 time steps of 1200 s) is shown in Fig. 3(c). Even though the bell has entered an area of higher resolution, with the focal point located just above the center of the plot, the error from the coarse grid area persists. In fact, the cumulative effect of the stretched solution is a doubling of the maximum error. Comparing with the initial height field, the profile has spread out in the same pattern the regular grid solution exhibits. Fig. 4 shows the comparison of the L_2 and $L_{\max}$ error norms as a function of time on the stretched and rotated grid and on the regular grids at T42. The increased accuracy around day two when the bell is traversing the high resolution area is seen as well as the degradation in accuracy when the bell is in the low resolution area of the sphere.

6.2. Zonal flow over an isolated mountain

Test Case 5 has no analytic solution, but it has been used to study different grid schemes because of the regional features of the solution. These features result from the zonal flow impinging on a single large mountain centered at $(\frac{3\pi}{2}, \frac{\pi}{6})$. This is the same location used for the focal point of the stretched grid. The surface mountain height is given by

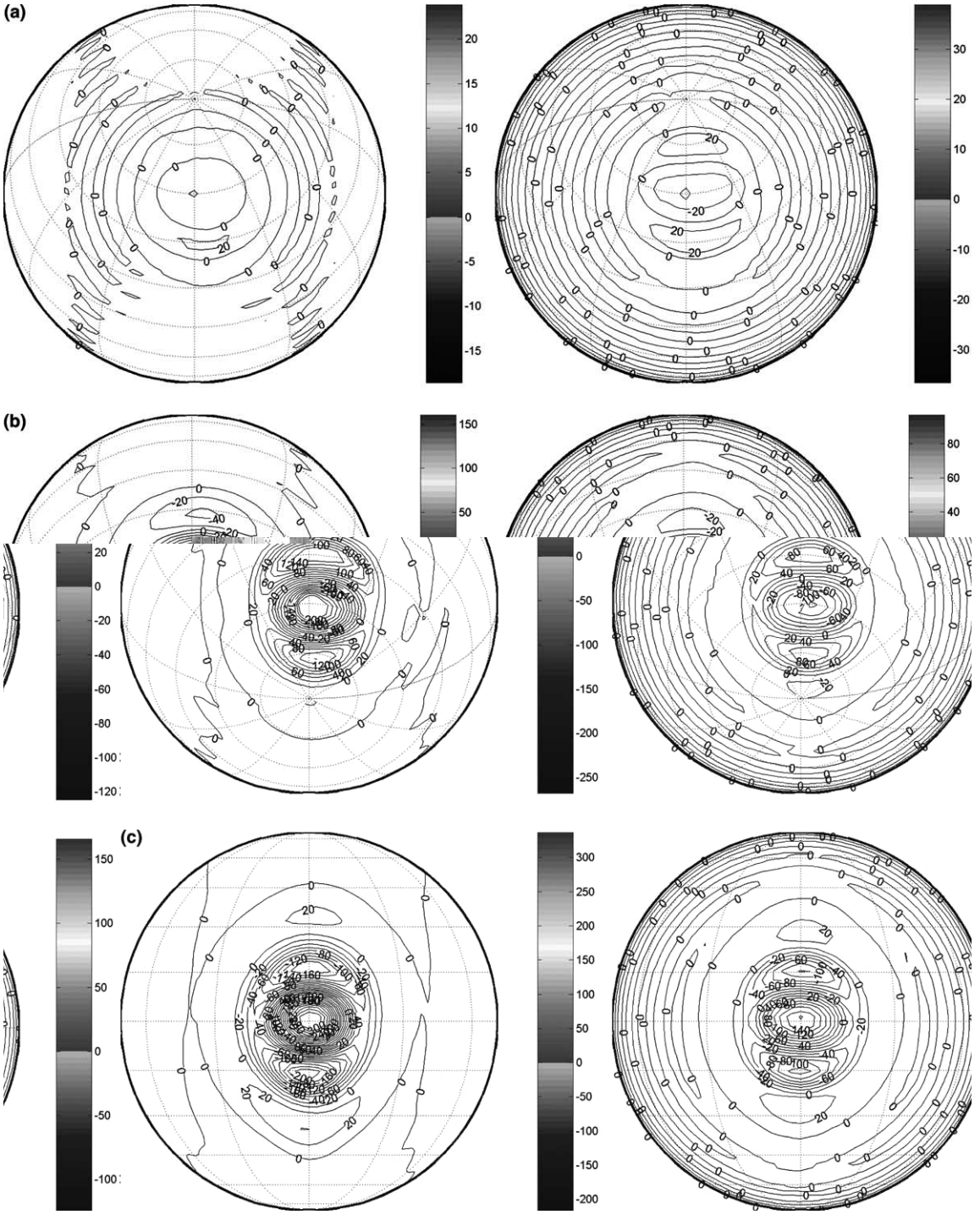

Fig. 3. Contour plots for Case 1 of the error in the height field at (a) day 2, (b) day 8, and (c) day 12 (one rotation). Left: on the stretched and rotated grids with the stretching factor 2 and focal point $(3\pi/2, \pi/6)$. Right: on the regular grids.

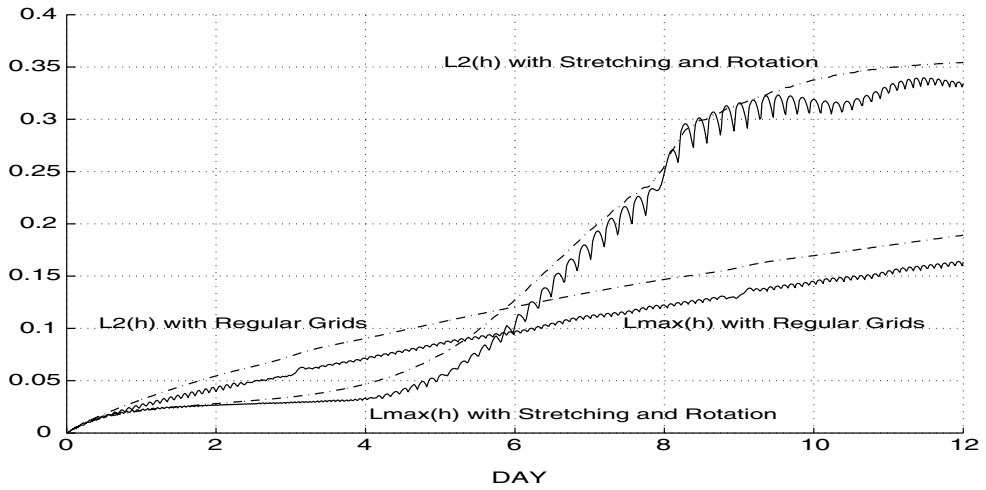

Fig. 4. Comparison for Case 1 of error norms in L_2 and L_∞ of height field on stretched ($c = 2$) and rotated ($3\pi/2, \pi/6$) grids and on regular grids.

$$h_s = h_{s_0}(1 - r/R),$$

where $h_{s_0} = 2000$ m, $R = \pi/9$ and $r^2 = \min[R^2, (\lambda - \lambda_c)^2 + (\theta - \theta_c)^2]$. The equivalent depth h_0 has been changed to 5960 m for this case.

The initial zonal flow defined from test Case 2 of [20] develops a lee wave with shedding vortices. The areas of sharpest gradient are above and in front of the mountain as seen in the contour plots of the height field shown in Fig. 5. The initial condition shows no effect of the surface orography while by day 5 (Fig. 5(a)), the wave structure has started to emerge. Each plot (at day 5, 10, and 15) of the series in Fig. 5 compares well with the reference solutions from an Eulerian spectral model given in [9]. The solutions are smooth and show improvement in the area of steepest gradients. The Eulerian spectral solutions show a "spectral ringing" just before the mountain which has been eliminated in the semi-Lagrangian formulation. The mechanism for the elimination of the spectral ringing is the inherent smoothing from the SLT interpolation.

In order to see the effect of stretching on the solution three simulations are compared in Figs. 6 and 7. The first figure is the difference of the solutions (T42) on regular grids and on stretched ($c = 2$) and rotated ($3\pi/2, \pi/6$) grids at 5 days. Clearly, the height fields are not the same. The area of largest change is in the focal area between $-60°$ and $-30°$. The focusing is refining the solution by resolving gradients in front of the mountain. The trend continues as the stretching factor is increased to $c = 3$ in Fig. 7.

Another effect of the focusing is a shift in the path of the downstream vortices as the mountain lee wave is better resolved. The difference plots in height show an increased smoothing away from the mountain in the coarse grid areas. Fig. 7 shows that the downstream height maximums are decreased with increased stretching because of this smoothing, though the effect is very small on the global solution.

Fig. 8 documents the changes in global mass and energy for Case 5 over the 15 day simulation period. The comparison shows the improvement of the results using the stretched grids. The stretched grids do a significantly better job in conserving total energy and mass. This may have implications for long time simulations where the stability of the calculation depends on accurately accounting for conserved quantities.

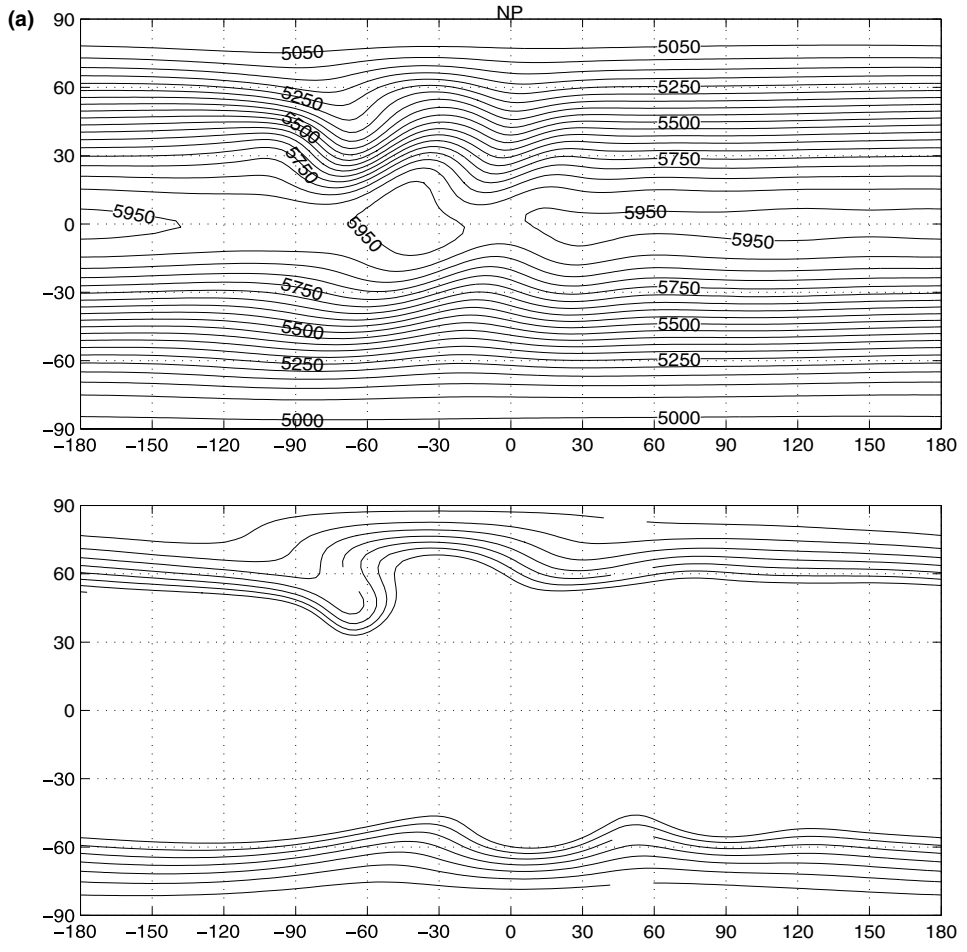
(a)
NP
90
60
30
0
−30
−60
−90
−180
−150
−120
−90
−60
−30
0
30
60
90
120
150
180
5050
5250
5500
5750
5950
5000

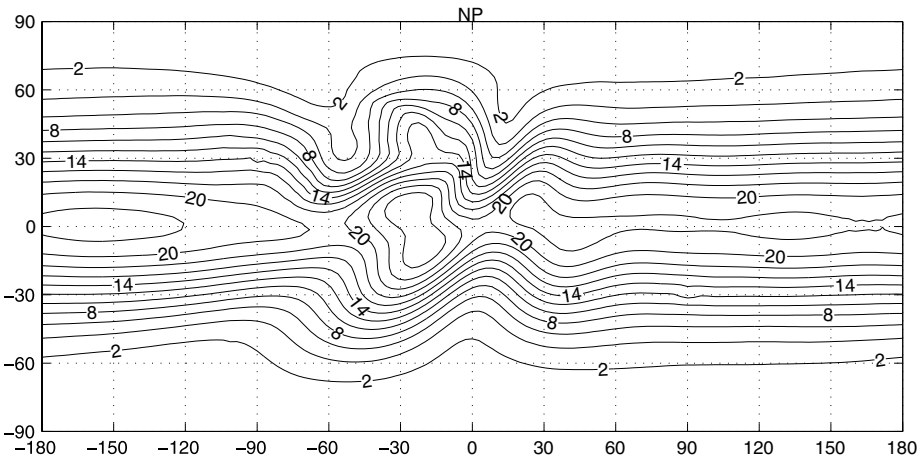

Fig. 6. Contour plot for Case 5 of the difference in height fields between regular grids and stretched ($c = 2$) grids at day 5.

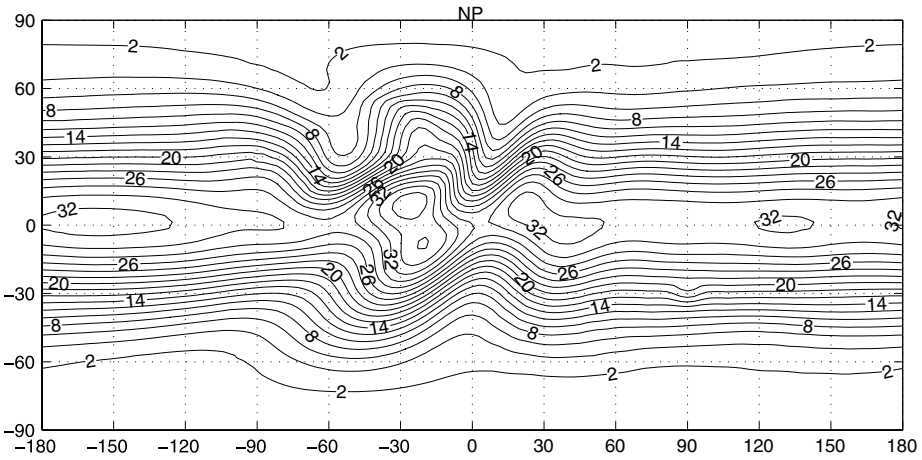

Fig. 7. Contour plot for Case 5 of the difference in height field between regular grids and stretched ($c = 3$) grids at day 5.

How the conservation is improved with the focused grid may be related to the conversion of potential and kinetic energies within the model. These conversions are most active in the area of high gradients of the geopotential, which are being better resolved and represented with the focused grid.

Fig. 9 shows the differences for the Case 5 on the regular grid of T85 and the stretched and rotated grid with the mapping factor $c = 2.5$ of T42. From the difference of the height fields, we got similar results around the mountain, where we have the focused grid of T42. In another words, we have doubled the resolution at the local area we are interested. However, in Fig. 10, we show the differences between the different time steps ($\Delta t = 1200$ s and $\Delta t = 3600$ s) on the regular grid of T85. The result shows the little impact of the big time step.

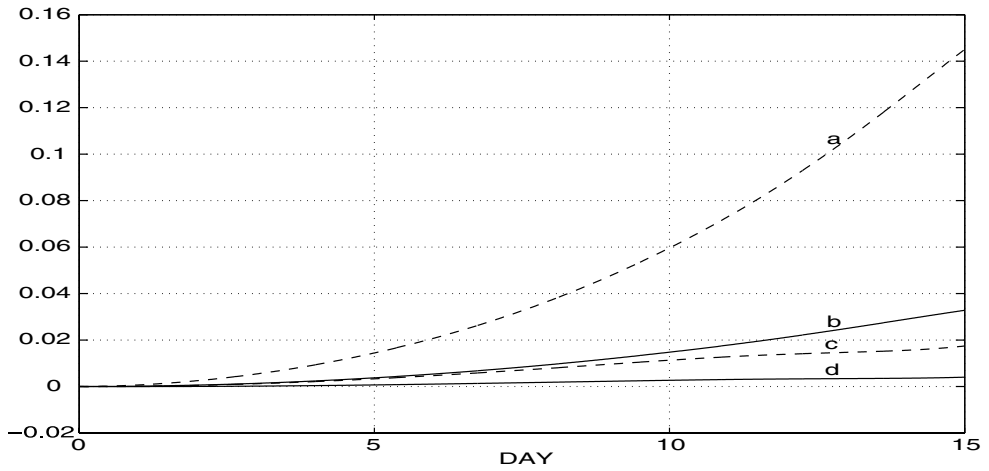

Fig. 8. Comparison for Case 5 of average relative changes of global mass (solid) and total energy (dash) on regular (a and b) and stretched rotated (c and d) grids.

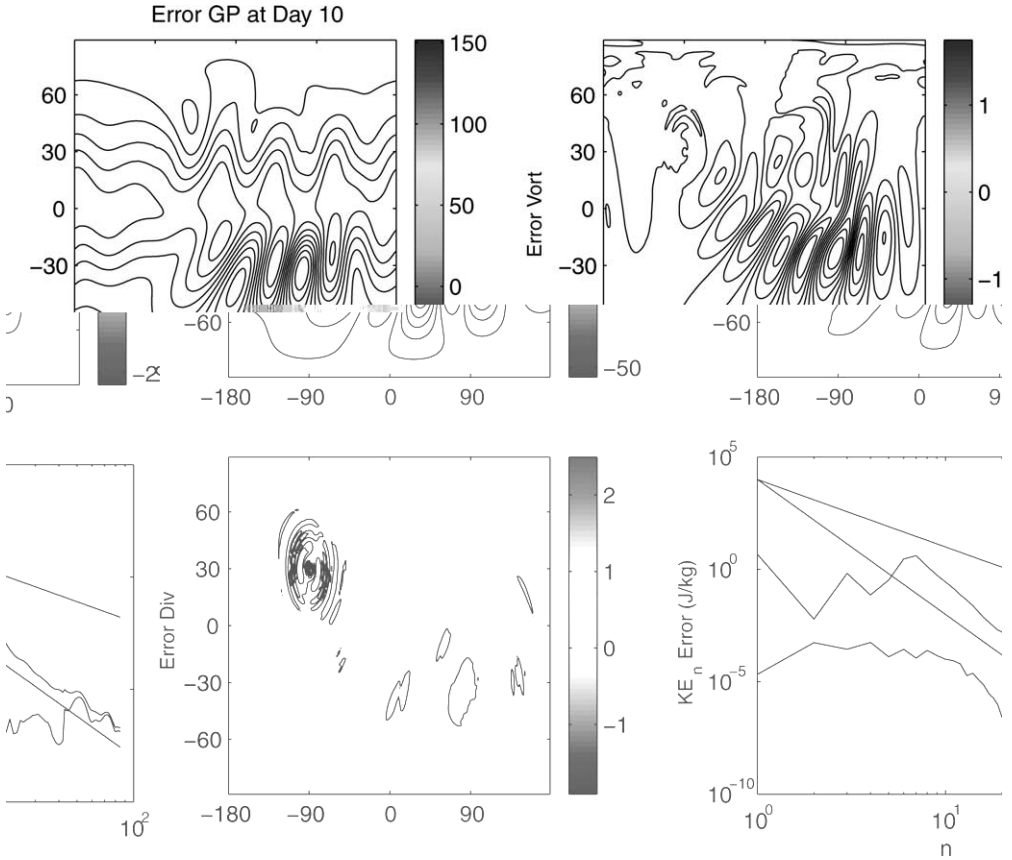

Fig. 9. Comparison for Case 5 between T85 on regular grid and T42 with $c = 2.5$. The time steps are $\Delta t = 1200$.

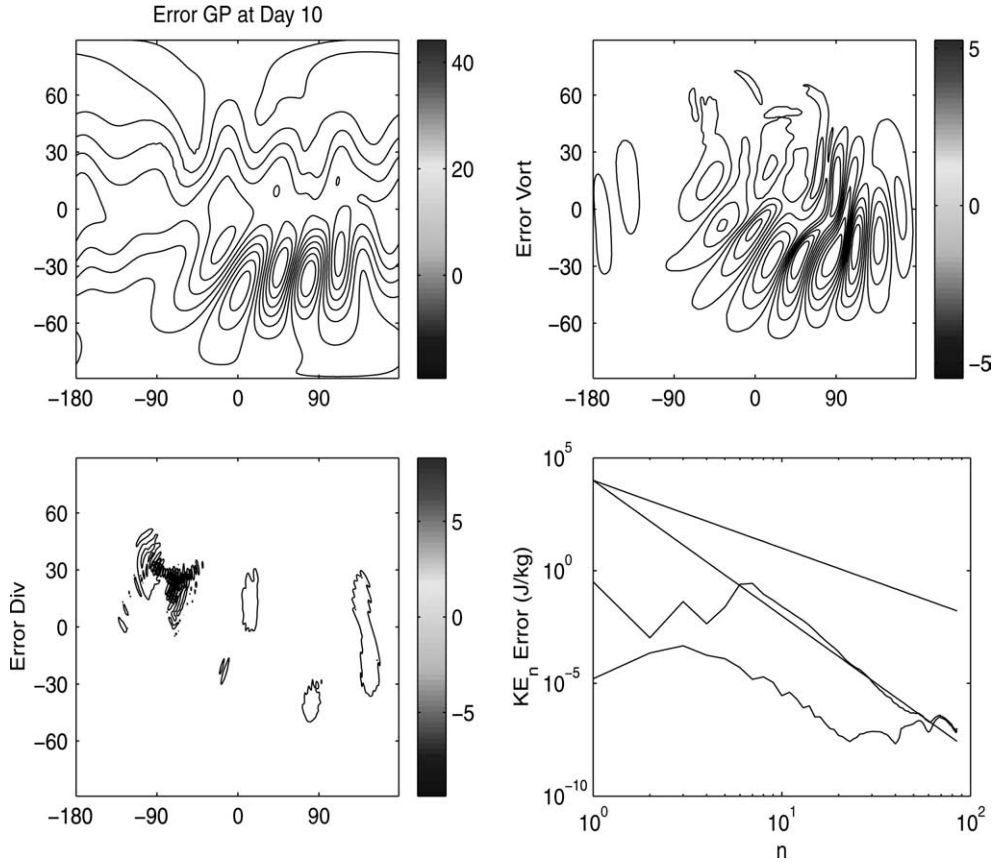

Fig. 10. Comparison for Case 5 (T85) on regular grids with $\Delta t = 1200$ and $\Delta t = 3600$.

7. Conclusions

The utility of focused grids to resolve special flow features has been investigated in the context of the shallow water equations in a spherical geometry. A vorticity–divergence formulation with an advective form suitable for the semi-Lagrangian transport scheme has been presented and shown to work effectively with a spectral discretization of the operators. The focused grids are based on Schmidt's conformal transformation and a suitable change of variables of the differential operators allows for a semi-implicit solution of the equations in spectral space.

The solutions of two shallow water test cases demonstrate the advantages of local resolution for certain types of weather and atmospheric flow phenomena. The accuracy and stability of the solutions compares favorably with a uniform Gaussian grid spectral formulation.

We have begun to extend the method with a generalization of the Schmidt mapping that will allow multiple regions to be resolved. A two-time level semi-Lagrangian formulation will also be examined to improve computational efficiency.

Acknowledgments

This research was supported by the Climate Change Prediction Program of the Climate Change Research Division, Office of Energy Research, US Department of Energy under contract DE-AC05-84OR21400 with UT-Battelle. Computing resources were provided by the Center for Computational Sciences-Climate and Carbon Research Institute at the Oak Ridge National Laboratory.

References

[1] J.R. Bates, F.H.M. Semazzi, R.W. Higgins, S.R.M. Barros, Integration of the shallow water equations on the sphere using a vector semi-Lagrangian scheme with a multigrid solver, MWR 118 (1990) 1615–1627.
[2] P. Coutier, J.F. Geleyn, A global numerical weather prediction model with variable resolution: application to the shallow-water equations, Quart. J. Roy. Meteor. Soc. 114 (1988) 1321–1346.
[3] J. Cote, A. Staniforth, A two-time-level semi-Lagrangian semi-implicit scheme for spectral models, MWR 116 (1988) 2003–2012.
[4] M. Deque, J.P. Piedelievre, High resolution climate simulation over Europe, Climate Dyn. 11 (1995) 321–339.
[5] J.B. Drake, D.X. Guo, A vorticity–divergence global semi-Lagrangian spectral model for shallow water equations, ORNL/TM-2001/216, 2001.
[6] D.X. Guo, J.B. Drake, A global semi-Lagrangian spectral model for the reformulated shallow water equations, in: Proceedings of 4th International Conference on Dynamics Systems and Differential Equations, 2002, pp. 375–385.
[7] J.J. Hack, R. Jakob, Description of a global shallow water model based on the spectral transform method, NCAR Technical Note NCAR/TN-343+STR, National Center for Atmospheric Research, Boulder, CO, 1992.
[8] V. Hardiker, A global numerical weather prediction model with variable resolution, MWR 125 (1997) 59–73.
[9] R. Jakob, J.J. Hack, D.L. Williamson, Spectral transform solutions to the shallow water test set, NCAR/0301/94-04, 1994.
[10] H. Ritchie, Application of the semi-Lagrangian integration scheme in a regional forecast model, MWR 113 (1985) 424–435.
[11] H. Ritchie, Application of the semi-Lagrangian method to a spectral model for the shallow water equations, MWR 116 (1988) 1587–1598.
[12] A. Robert, J. Henderson, C. Turnbull, An implicit time integration scheme for baroclinic models of the atmosphere, MWR 100 (1972) 329–335.
[13] F. Schmidt, Variable fine mesh in a spectral global model, Beitr. Phys. Atmos. 50 (1977) 211–217.
[14] F. Schmidt, Cyclone tracing, Beitr. Phys. Atmos. 55 (1982) 335–357.
[15] A. Staniforth, J. Côté, Semi-Lagrangian integration schemes for atmospheric models – a review, MWR 119 (1991) 2206–2223.
[16] P.N. Swarztrauber, Spectral transform methods for solving the shallow-water equations on the sphere, MWR 124 (4) (1996) 730–744.
[17] W.M. Washington, C.L. Parkinson, An Introduction to Three-Dimensional Climate Modeling, University Science Books, 1988.
[18] D.L. Williamson, P.J. Rasch, Two-dimensional semi-Lagrangian transport with shape-preserving interpolation, MWR 117 (1) (1989) 102–128.
[19] D.L. Williamson, J.D. Drake, J.J. Hack, R. Jakob, P.N. Swarztrauber, A standard test set for numerical approximations to the shallow water equations in sperical geometry, J. Comput. Phys. 102 (1992) 211–224.
[20] D.L. Williamson, J.G. Olson, Climate simulations with a semi-Lagrangian version of the NCAR Community Climate Model, MWR 122 (1994) 1594–1610.
[21] K. Yessad, P. Benard, Introduction of local mapping factor in the spectral part of the Metro-France global variable mesh numerical forecast model, Quart. J. Roy. Meteor. Soc. 122 (1996) 1701–1719.